Increased expression of system x_c^- in glioblastoma confers an altered metabolism and chemoresistance

Monika D. Polewski,

Department of Neurosciences, City of Hope National Medical Center and Beckman Research Institute, Duarte, California, 91010, USA

Irell and Manella Graduate School of Biological Sciences, City of Hope National Medical Center and Beckman Research Institute, Duarte, California, 91010, USA

Rosyli F. Reveron-Thornton,

Department of Neurosciences, City of Hope National Medical Center and Beckman Research Institute, Duarte, California, 91010, USA

Department of Biological Sciences, California State University, San Bernardino, California, 92407, USA

Gregory A. Cherryholmes,

Department of Cancer Immunotherapeutics and Tumor Immunology, City of Hope National Medical Center and Beckman Research Institute, Duarte, California, 91010, USA

Irell and Manella Graduate School of Biological Sciences, City of Hope National Medical Center and Beckman Research Institute, Duarte, California, 91010, USA

Georgi K. Marinov,

Division of Biology, California Institute of Technology, Pasadena, California, 91125, USA

Kaniel Cassady, and

Departments of Diabetes Research and Hematology/Hematopoietic Cell Transplantation, City of Hope National Medical Center and Beckman Research Institute, Duarte, California, 91010, USA

Irell and Manella Graduate School of Biological Sciences, City of Hope National Medical Center and Beckman Research Institute, Duarte, California, 91010, USA

Karen S. Aboody

Department of Neurosciences, City of Hope National Medical Center and Beckman Research Institute, Duarte, California, 91010, USA

Division of Neurosurgery, City of Hope National Medical Center and Beckman Research Institute, Duarte, California, 91010, USA

Correspondence: **Monika D. Polewski, Ph.D.,** Department of Neurosciences and Irell and Manella Graduate School of Biological Sciences, City of Hope National Medical Center & Beckman Research Institute, 1500 East Duarte Road, Duarte, CA 91010-3000, Tel: 619-395-5319; Fax: 626-471-7371; monika.polewski@gmail.com. **Karen S. Aboody, M.D.**, Department of Neurosciences and Division of Neurosurgery, City of Hope National Medical Center & Beckman Research Institute, 1500 East Duarte Road, Duarte, CA 91010-3000, Tel: 626-471-7177; Fax: 626-471-7371; kaboody@coh.org.

Abstract

Glioblastoma multiforme (GBM) is the most aggressive malignant primary brain tumor in adults. Several studies have shown that glioma cells up-regulate the expression of xCT (*SLC7A11*), the catalytic subunit of system x_c^-, a transporter involved in cystine import, that modulates glutathione production and glioma growth. However, the role of system x_c^- in regulating the sensitivity of glioma cells to chemotherapy is currently debated. Inhibiting system x_c^- with sulfasalazine decreased glioma growth and survival via redox modulation, and use of the chemotherapeutic agent temozolomide together with sulfasalazine had a synergistic effect on cell killing. To better understand the functional consequences of system x_c^- in glioma, stable *SLC7A11* knock-down and over-expressing U251 glioma cells were generated. Modulation of *SLC7A11* did not alter cellar proliferation but over-expression did increase anchorage-independent cell growth. Knock-down of *SLC7A11* increased basal ROS and decreased glutathione generation resulting in increased cell death under oxidative and genotoxic stress. Over-expression of *SLC7A11* resulted in increased resistance to oxidative stress and decreased chemosensitivity to temozolomide. In addition, *SLC7A11* over-expression was associated with altered cellular metabolism including increased mitochondrial biogenesis, oxidative phosphorylation and ATP generation. These results suggest that expression of *SLC7A11* in the context of glioma contributes to tumorigenesis, tumor progression, and resistance to standard chemotherapy.

Implications: *SLC7A11*, in addition to redox modulation, appears to be associated with increased cellular metabolism and is a mediator of temozolomide resistance in human glioma, thus making system x_C^- a potential therapeutic target in GBM.

Keywords

SLC7A11; glioma; oxidative stress; glutathione; chemoresistance; metabolism

Introduction

Glioblastoma multiforme (GBM), a grade IV astrocytoma, is the most common and aggressive primary brain tumor in adults; patient survival averages only 14 months after diagnosis (1). The standard-of-care for patients with newly diagnosed GBM includes aggressive safe tumor resection followed by radiotherapy with concomitant systemic chemotherapy using the alkylating agent temozolomide (TMZ) (2). Unfortunately, patients with high grade gliomas inevitably progress or relapse an average of only 6.9 months after treatment (3). Therapeutic options for recurrent GBM are limited and generally not effective. One of the main causes of treatment failure in GBM patients is resistance to post-operative radiation and chemotherapy. Many mechanisms contribute to the development of drug resistance, including DNA repair, drug uptake and efflux, apoptosis and glutathione-mediated cellular detoxification pathways (4). Thus, an improved understanding of the molecular mechanisms involved in glioma progression and survival, as well as mediators of TMZ resistance, could lead to development of more effective therapeutic strategies.

One of the mechanisms for chemo- and radiotherapy is to disproportionately increase intracellular reactive oxygen species (ROS) to induce cell cycle arrest, senescence and apoptosis (5). Accumulation of ROS can trigger apoptosis due to oxidative damage to DNA,

macromolecules, lipids and mitochondria. However, up-regulation of antioxidant systems is observed in various tumors making them more resistant to chemotherapy (6). Approaches to maximally exploit ROS-mediated cell death by combining drugs that induce ROS generation with compounds that suppress cellular antioxidant capacity have been proposed years ago (7).

System x_c^-, a sodium-independent membrane transporter, couples the influx of extracellular cystine to the efflux of glutamate (8). Expression of system x_c^-, specifically the catalytic domain xCT, is up-regulated in gliomas, and several studies have shown over-expression confers a growth advantage, either through increased extracellular glutamate levels that promote neuronal cell death or through increased import of cystine that is converted to cysteine (8–11). Cysteine is the rate-limiting precursor for generating the major antioxidant glutathione (GSH). GSH can neutralize intracellular ROS or be conjugated by glutathione S-transferases to xenobiotic agents, which are then exported out of the cell (12, 13).

There is accumulating evidence that GSH and system x_c^- may mediate resistance of cancer to cytotoxin-based therapies (5). Radiation therapy-resistant glioma cells exhibited a 5-fold increase in the expression of antioxidant enzymes such as superoxide dismutase, glutathione peroxidase, and glutathione reductase that maintain redox balance (14). High intracellular GSH levels in cancer cells have also been associated with drug resistance and detoxification of alkylating agents. System x_c^- has been shown to maintain intracellular GSH levels in ovarian cancer cells, resulting in cisplatin resistance (15). Inhibition of system x_c^- in pancreatic cancer cells led to growth arrest and over-expression led to gemcitabine resistance (16). Recent findings also support the hypothesis of a correlation between adaption to oxidative stress, low mitochondrial ROS, enhanced mitochondrial respiration and resistance to chemotherapy drugs (17).

In this study, we show that xCT (*SLC7A11*) was highly expressed in established glioma cell lines and that treating cells with sulfasalazine (SSZ), an inhibitor of system x_c^-, decreased glioma growth and increased ROS-mediated cell death. Inhibiting system x_c^- in U251 glioma cells with SSZ concomitant with TMZ treatment had a synergistic killing effect. However, stable knock-down of *SLC7A11* in U251 glioma cells did not alter cell growth or viability under basal conditions, despite changes in redox balance. Over-expression of *SLC7A11* resulted in anchorage-independence and resistance to oxidative stress, while *SLC7A11* knock-down decreased anchorage-dependent cell growth and resistance to oxidative stress. Knocking-down expression of *SLC7A11* in U251 glioma cells also increased their sensitivity to TMZ. In contrast, U251 cells in which *SLC7A11* was over-expressed had decreased sensitivity to TMZ and reduced apoptosis. Over-expression of *SLC7A11* in U251 glioma cells also resulted in an up-regulation of genes involved in cellular metabolism, increased mitochondrial biogenesis, oxidative phosphorylation, and ATP production while maintaining low cytoplasmic and mitochondrial ROS levels. These results suggest that high expression of *SLC7A11*/system x_c^- activity may confer resistance of glioma to TMZ treatment by increasing GSH production for redox balance and promoting cellular metabolism.

Materials and Methods

Cell Culture

Human glioma cell lines (U251 and U87) and normal primary human astrocytes (pNHA) were purchased from American Type Culture Collection (ATCC) and cultured as previously described (18). The primary high grade glioma line PBT017 was obtained and cultured as previously described (18). For genotoxic or oxidative stress studies, cells were treated 24 h after plating with either 300 μM TMZ for 72 h or 100 μM H_2O_2 for 6 h.

Orthotopic Transplantation and Histopathological Analysis

In vivo studies were carried out in an orthotopic U251, U87, and PBT017 human glioma mouse model. Tumors were established by stereotactic, intracranial injection of 2×10^5 cells into the frontal lobe of NOD-scid mice. At 4 weeks, mice were perfused transcardially with 4% paraformaldehyde in PBS. Brains were harvested and formalin-fixed paraffin-embedded sections were stained with hematoxylin-eosin to confirm the presence of tumors. To assess xCT protein expression *in vivo*, sections were incubated overnight with a goat anti-human polyclonal xCT antibody (LS-B4345, LifeSpan Biosciences, Inc.) followed by incubation with secondary antibodies conjugated to horseradish peroxidase and detected using a DAB Peroxidase Substrate Kit (Vector Laboratories, Inc.)

RNA Isolation, cDNA Synthesis, and Quantitative Real-time-PCR

Total RNA was extracted using Trizol reagent. Synthesis of cDNA was performed using the BioRad cDNA synthesis kit. SYBR green PCR master mix (Life Technologies) was used for quantitative real-time PCR (qRT-PCR) monitored with a C1000 Thermal Cycler (BioRad) as previously described.(19) Reaction conditions for qRT-PCR were as follows: 1 cycle of 3 min at 95ºC; 39 cycles of 10 s at 95ºC, 10 s at 55ºC, 30 s at 72 ºC; 1 cycle of 10 s at 95°C; and a melting curve of 5 s at 65°C - 95°C. A standard linear curve was generated using pooled sample DNA and the threshold exponential amplification cycle (C_T) was calculated by system software. The following primer sequences were used: human *SLC7A11*: 5'-CTGAGGAGCTGCTGCTTTCAAA-3' and 5'-AGGAGAGGGCAACAAAGATCGGAA-3'; and human *GAPDH*: 5'-ACCAAATCCGTTGACTCCGACCTT-3' and 5'-TTCGACAGTCAGCCGCATCTTCTT-3'.

Western Blot Analysis

Total protein extraction and Western blot analysis were performed as previously described. (9) The following primary antibodies were used: polyclonal goat anti-xCT (GTX89082; GeneTex), and rabbit monoclonal anti-active caspase-3 (ab32042; Abcam). Immunoreactivity was detected with a polyclonal rabbit-anti goat horseradish peroxide (HRP)-conjugated secondary antibody, and a polyclonal rabbit-anti goat HRP-conjugated secondary antibody, respectively. Mouse β-actin (A1978; Sigma-Aldrich) was used as a loading control and detected with polyclonal goat- anti mouse HRP- conjugated secondary antibody (Cat. 1706516; BioRad).

Immunofluorescence Microscopy

Cells were fixed with 4% paraformaldehyde and stained with a rabbit polyclonal antibody to xCT (NB-300–318; Novus Biologics). Immune complexes were detected with an AlexaFlour-488 conjugated secondary antibody (Molecular Probes). Nuclei were counterstained with DAPI (Vectastain). Images were acquired with a LSM 510 Meta Inverted 2-photon confocal microscope.

Production of shSLC7A11 and SLC7A11 U251 Glioma Cell Lines

Lentivirus particles were produced by transfection of HEK 293T cells with either 15 μg of human TRC-pLKO.1-*SLC7A11* shRNA (TRCN0000043123, TRCN0000043125, TRCN0000043126, TRCN0000288865, or TRCN0000380471), 15 μg of pLK01-non-targeting shRNA (Mission shRNA, Sigma-Aldrich) or 15 μg of a human *SLC7A11*-pLX304 plasmid (DNASU Plasmid Repository) using calcium phosphate coprecipitation. The culture medium was replaced with fresh 10% FBS in 1xDMEM after 8 h and supernatant was collected 48 h after transfection. After determination of viral titers, U251 cells were incubated with a viral vector containing the appropriate over-expressing RNA, shRNA, or control shRNA, using a multiplicity of infection of 0.5. Blasticidin (1.0 μg/mL) (Sigma-Aldrich) or puromycin (10 μg/mL) (Sigma-Aldrich) selection was used to obtain stable recombinant *SLC7A11* over-expressing and sh*SLC7A11* knock-down U251 cells, respectively. Parental U251 cells served as controls for *SLC7A11* over-expressing cells while cells transduced with an empty vector served as controls for the *SLC7A11* knock-down cells.

ROS Production

Production of intracellular ROS under basal and treatment conditions was measured using the cell-permeant 2',7'-dichlorodihydrofluorescein diacetate (H_2DCFDA) (Invitrogen). To evaluate the direct production of mitochondrial ROS in cells, MitoTracker Red CM-H_2XRos, which is dependent on the mitochondria membrane potential (Ψ_m), was used. At the indicated time-points, cells were incubated (6% CO_2, 37ºC, 30 min) with either 5μM H_2DCFDA or 500 nM MitoTracker Red. Media was aspirated; cells collected with Accutase and spun down at 1200 x g for 5 min. Cells were then resuspended in flow buffer (1% FBS in PBS) and analyzed using a BD Accuri C6 Flow Cytometer.

Glutamate Measurement

Glutamate was measured in media samples using the BioProfile 100 Plus (Nova Biomedical). *SLC7A11* modified and control U251 cells were cultured in glutamate free DMEM for 24 h. After culture, 600 μL of media was removed from each sample dish and analyzed according to the manufacturer's instructions.

Assessment of Mitochondria Function

Mitochondrial function was examined by staining with the mitochondrial membrane potential (Ψ_m)-sensitive fluorochrome MitoTracker Red CMXRos. Cells (200,000 cells/well) were plated (12-well plate), cultured overnight, and then incubated (60 minutes, 37ºC) with 500 nM of MitoTracker Red CMXRos. After two washes with PBS, cells were fixed

with methanol:acetone (3:1) for 10 min. Cells were washed twice in PBS, mounted in Dako Fluorescent Mounting Medium and imaged on a LSM 510 Meta Inverted 2-photon confocal microscope.

Measurement of Apoptosis

Apoptosis ratios were analyzed using the Alexa Fluor 488 AnnexinV/Dead Cell Apoptosis kit (Invitrogen) according to the manufacturer's instructions. Samples were analyzed on a BD Accuri C6 Cytometer, and Annexin V$^-$/ PI$^-$ cells were used as unstained controls.

Quantification of Total Cellular ATP

To measure intracellular ATP, cells were lysed in buffer (200 mM Tris, 2 mM EDTA, 150 mM NaCl, 0.5% Triton X-100) and CellTiter-Glo Luminescence Viability Assay (Promega) was performed according to the manufacturer's protocol. An ATP standard curve was generated by serial dilutions of a 1 mg ATP stock (Sigma Aldrich). Luminescence measured using a SpectraMax M3 (Molecular Devices).

Glutathione Measurement

At the indicated time-points, cells were lysed with 200 µl of MES buffer (0.4 M 2-(N-morpholino) ethanesulphonic acid, 0.1 M phosphate, 2 mM EDTA, pH 6.0) and sonicated. Protein concentrations were quantified using the BCA Protein Assay (Thermo Scientific). A Glutathione Assay Kit (Caymen Chemical) was used to quantify total GSH and glutathione disulfide (GSSG) according to manufacturer's protocol. Absorbance was measured at 405 nm using a SpectraMax M3.

Cell Viability and Proliferation Assays

Cell counting kit-8 (CCK-8; Dojindo Molecular Technologies) was used to measure cell viability according to the manufacturer's protocol. Absorbance was measured at 450 nm using a SpectraMax M3. A colorimetric immunoassay (Roche Diagnostics) was used according to the manufacturer's protocol to quantify cell proliferation based on the measurement of BrdU incorporation during DNA synthesis. Absorbance was measured at 370 nm using a SpectraMax M3. Cell numbers at each time-point were determined by flow cytometry (Guava EasyCyte, Millipore) using Guava Viacount (Millipore).

Soft Agar Assay for Anchorage-Independent Cell Growth

Anchorage-independent growth was determined by seeding 2.5×10^4 cells per 12 well in 0.35% agar on top of a base layer containing 0.4% agar. Plates were incubated at 37 °C at 5% CO_2 in a humidified incubator for 30 days and stained with 0.005% crystal violet for 1 h. Colonies >0.1 mm in diameter were counted under a microscopic field at ×10 magnifications.

Transmission Electron Microscopy

Cultured cells were pelleted and cryo-fixed in a Leica EM PACT2 high pressure freezer (~2,000 bars). In a Leica automated freeze substitution system AFS2, cryo-fixed specimens were freeze-substituted in anhydrous acetone containing 2% osmium tetroxide. The

temperature progression was 8 h at –90°C, –90°C to –60°C at 5°C/h, –60°C for 16 h, –60°C to 0°C at 5°C/h. Cells were held at 0°C until time for further processing, when they are warmed to room temperature, rinsed in pure acetone, infiltrated and embedded in Epon812 at 60°C for 48 hours. Ultra-thin sections (~70 nm thick) were cut using a Leica Ultra cut UCT ultramicrotome with a diamond knife, picked up on 200 mesh nickel EM grids. For morphology, grids were stained with 2% uranyl acetate in 70% ethanol for 1 minute followed Reynold's lead citrate staining for 1 minute. Electron microscopy was done on an FEI Tecnai 12 transmission electron microscope equipped with a CCD camera.

Oxygen Consumption and Extracellular Acidification Rate

Oxygen consumption rate (OCR) and extracellular acidification rate (ECAR) was determined using XF24 Extracellular Flux analyzer (Seahorse Bioscience, North Billerica, MA). Briefly, cells (20,000/well) were plated into XF24 polystyrene cell culture plates (Seahorse Bioscience) and incubated for 24 hours in a humidified 37°C incubator with 10% CO_2 (DMEM medium with 10%FBS). The following day, cells were washed, fresh assay media (2mM L-Glutamine + 2mM Pyruvate + 25mM Glucose in XF Base Media; pH to ~7.35) was added and cells incubated in a 37°C/non-CO_2 incubator for 60 minutes prior to the start of an assay. Sensor cartridges were calibrated and loaded to dispense three metabolic inhibitors sequentially at specific timepoints: oligomycin (inhibitor of ATP synthase, 8uM/port), followed by FCCP (a protonophore and uncoupler of mitochondrial oxidative phosphorylation, 18uM/port), followed by the addition of rotenone (mitochondrial complex I inhibitor, 25uM/port). Basal OCR and ECAR were measured, as well as changes in oxygen consumption caused by the addition of the metabolic inhibitors described above. Cells were treated with trypsin and then counted to determine the cell number in each well after the assay. OCR and ECAR were reported as normalized rates (pmoles/cell for OCR and mpH/cell for ECAR) or expressed as a percentage of the baseline oxygen consumption. Each datum was determined minimally in replicates of five. Several parameters were deducted from the changes in oxygen consumption including ATP turnover, proton leak, maximal respiratory capacity, and mitochondrial reserve capacity (= [maximum mitochondrial capacity] – [basal OCR]).

RNA-Sequence Data Generation and Analysis

Sequencing libraries were prepared with TruSeq RNA Sample Preparation Kit V2 (Illumina, San Diego) according to the manufacturer's protocol with minor modifications. Briefly, 500 ng of total RNA from each sample was used for polyadenylated RNA enrichment with oligo dT magnetic beads, and the poly(A) RNA was fragmented with divalent cations under elevated temperature. First-strand cDNA synthesis produced single-stranded DNA copies from the fragmented RNA by reverse transcription. After second-strand cDNA synthesis, the double-stranded DNA underwent end repair, and the 3′ ends were adenylated. Finally, universal adapters were ligated to the cDNA fragments, and 10 cycles of PCR were performed to produce the final sequencing library. Library templates were prepared for sequencing using cBot cluster generation system (Illumina) with TruSeq SR Cluster V3 Kit. Sequencing run was performed in single read mode of 51 cycle of read1 and 7 cycles of index read using Illumina HiSeq 2500 platform with TruSeq SBS V3 Kits. Real-time analysis (RTA) software was used to process the image analysis and base calling.

Sequencing runs generated approximately 40 million single reads for each sample. The refSeq annotation for the hg19 version of the human genome was used to create a transcriptome Bowtie (20) index (version 0.12.7), to which reads were aligned with the following settings: "-v 3 -a". Gene expression levels were estimated using eXpress (21) (version 1.4.1), and the effective count values were used as input to DESeq (22) for evaluating differential expression.

Statistical Analysis

Experiments were performed in at least triplicate and repeated at least three independent times. Statistical significance was determined by difference of means between two groups and was calculated using Student's *t* test. All reported p-values were two-sided; P<0.05 was considered significant.

Results

SLC7A11/xCT is Up-regulated in Glioma Cell Lines and Inhibition Induces ROS-Mediated Cell Death

The expression of *SLC7A11* and xCT in human astrocytoma cell lines was assessed by qRT-PCR and Western blot analysis, respectively. Both the U87 and U251 established astrocytoma cell lines had greater *SLC7A11* gene (Fig. 1A) and xCT protein expression (Fig. 1B) as compared to primary normal human astrocytes (pNHAs). Protein expression was also retained when U87 and U251 cells or a primary high grade glioma line, PBT017, were orthotopically transplanted into NOD-scid mice (Fig. 1C).

To determine if system x_c^- transport activity is necessary for the survival of glioma cells, we treated U251 glioma cells with increasing doses of the pharmacologic inhibitor SSZ. BrdU incorporation, which is a relative measure of cellular proliferation, showed a dose-dependent decrease with higher SSZ doses (1000 μM and 1500 μM) at multiple time points (Suppl. Fig 1A). After 72 h of SSZ treatment, there was a dose-dependent decrease in U251 cell numbers (Fig. 1D). A majority of the cells were lost at the higher doses for the cell count assay; therefore we chose to use 500 μM SSZ for subsequent assays. To determine whether the decrease in cell growth was due to apoptosis, Annexin V-PI staining was performed. Treatment of U251 cells with 500 μM SSZ resulted in a large increase in apoptotic cells (Suppl. Fig 1B). We also reasoned that inhibiting system x_c^- transport activity should result in decreased amounts of intracellular antioxidants (e.g., cysteine and GSH), and a subsequent increase in pro-oxidants. Intracellular ROS levels were measured by DCF staining to determine if there was a more pro-oxidant state that could contribute to the increased cell death observed after SSZ treatment. Indeed, treatment of the glioma cells with 500 μM SSZ resulted in significantly greater amounts of intracellular ROS compared to non-treated cells (Fig. 1E).

Synergistic Cytotoxicity in Glioma between the Chemotherapeutic Agent Temozolomide and an Inhibitor of System X_c^-

We evaluated whether inhibition of system x_c^- could change the chemosensitivity or chemoresistance of U251 cells to TMZ, the standard chemotherapeutic agent used to treat

newly diagnosed GBM patients. We first examined whether pharmacologically inhibiting system x_c^- with SSZ would increase the toxicity of TMZ. Parental U251 cells were treated for 3 days with increasing doses of SSZ (50, 100, 200, 400, 800, or 1600 μM) and increasing doses of TMZ (12.5, 25, 50, 100, 200, 400, or 800 μM). A combination index (CI)-isobologram equation was used to quantitatively determine drug interactions, where CI<1 indicates synergism, 1 indicates an additive effect, and >1 indicates antagonism (23). A synergistic effect was seen with all doses of TMZ and 50 μM of SSZ as well as other lower doses of both drugs (Fig. 1F), indicating that inhibition of system x_c^- may sensitize glioma cells to chemotherapy. SSZ doses at 800 μM or higher showed additive or antagonistic effects.

SLC7A11 Over-expression Confers Resistance to Oxidative Stress

To gain insight in the function of *SLC7A11* in human glioma, we established stable U251 over-expressing and knock-down lines using lentiviral vector-mediated gene transfer and RNA silencing technology. The *SLC7A11* over-expressing cells expressed 10-fold more *SLC7A11* mRNA than did control cells (Fig. 2A), and this was accompanied by greater xCT protein expression, as shown by Western blot analysis (Suppl. Fig. 2A) and immunocytochemistry (Fig. 2B). Five different shRNA clones to target different regions of *SLC7A11* were tested to obtain the most efficient knock-down compared to empty vector control. Because the sh*SLC7A11*_ TRCN0000043126 construct suppressed gene and total protein expression the most in the transduced U251 cells (Suppl. Fig. 2B), which was confirmed by immunocytochemistry (data not shown), we chose it for further analysis. The *SLC7A11*-knock-down cell expressed significantly less *SLC7A11* mRNA than did the cells transduced with an empty vector (Fig. 2A) Knock-down of xCT (*SLC7A11*) protein expression was confirmed by immunocytochemistry (Fig. 2B).

To assess whether modification of *SLC7A11* expression affects system x_c^- transport activity, we measured glutamate release into the media. *SLC7A11* over-expressing cells released significantly more glutamate compared to control cells, while *SLC7A11*-knock-down cells released significantly less, indicating the cystine influx: glutamate efflux transporter was functional (Fig. 2C). We found that enhancement or suppression of *SLC7A11* expression in established cell lines did not influence cell proliferation (Fig. 2E) or cell viability (Fig. 2F). However, a soft agar assay revealed that the *SLC7A11* over-expressing cells had higher anchorage-independent cell growth while the *SLC7A11* knock-down cells had lower anchorage-independent cell growth, indicating that the *SLC7A11* over-expressing cells may be more tumorigenic (Fig. 2D).

Because system x_c^-, or more specifically its catalytic subunit xCT, plays an important role in regulating GSH levels, we evaluated intracellular GSH and ROS in the *SLC7A11*-modified U251 lines. Under basal conditions, the *SLC7A11* knock-down cells had significantly lower intracellular GSH levels as compared to their respective controls (Fig. 3A), and this correlated with significantly higher intracellular ROS levels (Fig. 3B). Although the *SLC7A11* over-expressing U251 cells did not have higher total intracellular GSH levels than the control, despite increased xCT expression, they did have significantly lower intracellular ROS levels under basal conditions (Fig. 3B). However, under oxidative stress conditions,

mimicked by treatment with 100 μM H_2O_2, the *SLC7A11* over-expressing cells had significantly increased intracellular GSH levels as compared to under basal conditions and to control cells treated with H_2O_2 (Fig. 3C). Consistent with increased GSH levels, H_2O_2-treated *SLC7A11* over-expressing cells showed markedly less H_2O_2-induced intracellular ROS (Suppl. Fig. 3) and less H_2O_2-induced apoptosis compared to control cells (Fig. 3D).

SLC7A11 Over-expression Confers Resistance to Genotoxic Stress Induced by Temozolimide

Various types of cancer exhibit elevated GSH levels, which makes these cancers more resistant to chemotherapy (6). The combinatorial drug studies indicated that inhibition of system x_c^- with SSZ could increase cell killing with TMZ under low doses. We next examined whether genetic manipulation of *SLC7A11* could modulate chemosensitivity to TMZ. The *SLC7A11* over-expressing cells had greater viability than did control cells treated with increasing doses of TMZ, while the *SLC7A11* knock-down cells were less viable than control cells (Fig. 4A). Consistent with this, the *SLC7A11* over-expressing cells had a 6-fold higher IC_{50} value for TMZ (419 μM) as compared to control cells (64 μM). The increased resistance to TMZ upon *SLC7A11* over-expression was further confirmed by higher cell proliferation rates compared to the control cells (Fig. 4 B). In addition, the *SLC7A11* over-expressing cells exhibited much less TMZ-induced apoptosis when treated than did control cells, while the *SLC7A11* knock-down cells showed a large increase in the percent of apoptotic cells (Suppl. Fig. 4A). To further test whether *SLC7A11* confers resistance to TMZ by inhibiting apoptosis, we analyzed expression of cleaved caspase-3, a marker of apoptotic cells, by Western blot analysis. Expression of cleaved caspase-3 was markedly greater in all TMZ-treated cell lines, but was lower in the *SLC7A11* over-expressing cells as compared to the *SLC7A11* knock-down cells (Fig. 4C). To determine whether increased GSH levels contributed to the increased chemoresistance of the *SLC7A11* over-expressing cells, we measured intracellular GSH levels cells exposed to 300 μm TMZ. Consistent with the effect of oxidative stress on increasing GSH levels (Fig. 3C) in *SLC7A11* over-expressing cells, the genotoxic stress induced by TMZ resulted in a significant increase in intracellular GSH levels (Fig. 4D). TMZ treatment of the *SLC7A11* knock-down cells did not alter GSH levels as compared to untreated cells (Suppl. Fig. 4B).

Differential Gene Expression in SLC7A11 Over-expressing and Knock-down Glioma Cells

RNA-sequence analysis was performed to assess gene expression changes upon *SLC7A11* over-expression and knock-down in U251 glioma. Differential expression analysis revealed over 4,000 differential genes between *SLC7A11* over-expression and respective control cells (Fig. 5A and Fig. 5B), and over 3,000 differential genes when *SLC7A11* is knocked down in U251 cells (Fig. 5A and Suppl. Fig. 5A). Gene Ontology (GO) enrichment analysis shows the number of GO terms that are over-represented (or under-represented) in the *SLC7A11* over-expressing glioma (Fig. 5C) and in the *SLC7A11* knock-down glioma compared to respective controls (Suppl. Fig. 5B), with a complete list of enriched categories included in the Supplementary Files. Representative GO terms indicate that several genes involved in mitochondrial biogenesis and mitochondrial function are up-regulated in the *SLC7A11* over-expressing glioma (Figure 5C), suggesting that *SLC7A11* over-expressing U251 cells may have altered metabolic function.

SLC7A11 Over-expressing Cells have Increased Mitochondrial Biogenesis

Morphological examination of mitochondria was performed utilizing a transmission electron microscope (TEM). The electron micrographs revealed relatively well-preserved mitochondria in the *SLC7A11* modified and control cells (Fig. 6A). Magnification of the mitochondria (right panel of each set) shows typical double membranes, the intermembrane space, cristae, and a matrix. Quantification of the mitochondria in the cell lines reveals that the *SLC7A11* over-expressing glioma has significantly higher number of mitochondria present compared to control cells (Fig. 6B), indicating that there is increased mitochondrial biogenesis. To further confirm increased mitochondria number and assess mitochondrial function, cells were stained with the mitochondrial membrane potential Ψ_m-sensitive fluorochrome, MitoTracker Red CMXRos. Fluorescent microscopic examination revealed a stronger MitoTracker Red CMXRos stain in the *SLC7A11* over-expressing glioma (Fig. 6C). Analysis of the mean fluorescence intensity showed significantly higher MitoTracker Red CMXRos stain in the *SLC7A11* over-expressing glioma compared to control cells (Fig. 6D). The increased accumulation and retention of the probe indicates higher mitochondrial membrane potential (Ψ_m) in the *SLC7A11* over-expressing glioma.

SLC7A11 Over-expressing Cells have Increased Oxidative Phosphorylation

To assess cellular bioenergetics in the *SLC7A11* over-expressing U251 cells, extracellular flux analysis was used to determine the oxygen consumption rate (OCR) which is a measurement of mitochondrial respiration. Basal respiration was significantly higher in the *SLC7A11* over-expressing U251 glioma compared to control cells (Fig. 7A). Basal respiration is usually controlled by ATP turnover and only partly by substrate oxidation and proton leak (24). Therefore, we next examined ATP turnover by inhibiting ATP synthase using oligomycin. Treatment with oligomycin revealed that the *SLC7A11* over-expressing cells had higher ATP-linked respiration (oligomycin-sensitive fraction) compared to control cells (Fig. 7B). The maximal respiratory capacity was measured in the presence of carbonyl cyanide-p-trifluoromethoxyphenyl-hydrazon (FCC), an uncoupler that causes dissipation of the proton gradient by carrying protons across the inner mitochondrial membrane (17). FCCP causes rapid depolarization of mitochondria and acceleration of electron flux through the electron transport chain which resulted in significantly higher mitochondrial oxidative capacity in the *SLC7A11* over-expressing glioma compared to parental U251 cells (Fig. 7C). The spare respiratory capacity is the ability of substrate supply and electron transport to respond to an increase in energy demand, and, therefore, maintenance of some spare respiratory capacity is a major factor defining cell survival (24). Although not statistically significant, the *SLC7A11* over-expressing U251 glioma had increased reserve capacity (p=0.058) compared to the control cells (Fig. 7D). Together these data suggest that the *SLC7A11* over-expressing glioma, which display higher basal OCR, ATP-linked respiration, mitochondrial oxidative capacity and spare respiratory capacity, have higher oxidative phosphorylation. Since mitochondria are one of the main producers of ROS and the primary producers of ATP, we performed analysis of ATP generation in the *SLC7A11* over-expressing cells. Consistent with the OCR data, *SLC7A11* over-expressing cells generate more ATP compared to control cells (Fig. 7E). Despite the increased ATP generation, the *SLC7A11* over-expressing cells had lower mitochondrial ROS compared to the *SLC7A11* knock-down cells or the control cells (Fig. 7F).

Discussion

It has been suggested that system x_c^- may be a promising cancer target since it may sensitize tumors to conventional chemo/radiation-based therapies by lowering GSH levels (25). One of the causes of post-operative radiation and chemotherapy treatment failure in GBM patients is an increase in GSH levels that may decrease chemotherapy-associated oxidative stress and play a role in glutathione-mediated cellular detoxification pathways. In this work, we have expanded on the role system x_c^- plays in TMZ resistance in human glioma and have identified a novel mechanism that may contribute to glioma progression, via metabolic alteration. Inhibitors of system x_c^-, such as SSZ, have been put forward as possible effective therapeutic options. SSZ has been shown to deplete GSH levels by inhibiting the uptake of cystine, which lowers levels of intracellular cysteine, the rate-limiting precursor for GSH synthesis (8).

Supporting use of system x_c^- inhibitors, we show that SSZ treatment of U251 glioma resulted in ROS-mediated cell death. In addition, SSZ treatment in combination with TMZ treatment had a synergistic killing effect in U251 glioma cells. By inhibiting system x_c^- using SSZ, the efficacy of TMZ was increased at lower doses *in vitro*. Other pharmacological inhibitors of xCT, such as erastin, have been shown to sensitize glioma cells to TMZ (26). This suggests that use of specific system x_c^- inhibitors could have promise for avoiding or greatly reducing TMZ-associated toxicity in GBM patients. However, other factors contributing to the decreased cell growth and viability cannot be ruled out since SSZ has been noted to target several other pathways (27). SSZ has several immunomodulatory effects, including inhibition of NF-κB, and inhibition of GSH S-transferase, which is responsible for conjugating GSH to xenobiotics for detoxification (28). These off-target effects limit the conclusions drawn from SSZ inhibition studies of system x_c^- in glioma cells. Clinical trials studying the effects of SSZ for the treatment of malignant glioma in adults were terminated due to adverse events and toxicity (29).

We circumvented the problems associated with SSZ inhibition of system x_c^- by generating stable *SLC7A11* knock-down and over-expressing U251 cell lines in order to better understand the role system x_c^- plays in glioma progression. In contrast to reports that inhibition of system x_c^- with SSZ led to decreased growth and cell cycle progression in glioma (8), we did not observe any changes in proliferation in the *SLC7A11*-modified lines. One possibility is that system x_c^- does not directly modulate cell growth and previous reports of transporter inhibition did not take into account the off-target effects associated with SSZ use. In addition, it is possible that the *SLC7A11* knock-down cells are able to take up enough cystine to support proliferation, whereas a complete *SLC7A11* knock-out would decrease glioma viability and growth. Although proliferation of the *SLC7A11* knock-down cells was not affected, their cystine uptake was impaired as evidenced by the significant decrease in glutamate release and GSH generation, and significant increase in intracellular ROS. In terms of resistance to oxidative stress, over-expression of *SLC7A11* conferred increased resistance to apoptosis, which we attributed to a significant increase in GSH generation. This suggests that the primary role of system x_c^- is in redox regulation rather than protein synthesis.

Because elevated GSH levels in cancer cells have been associated with drug resistance, we hypothesized that system x_c^- may play a role in modulating genotoxic stress induced by TMZ. We found that over-expression of *SLC7A11* reduced the sensitivity of glioma to TMZ and decreased TMZ-induced apoptosis. Disruption of system x_c^- function by knocking down *SLC7A11* expression to low levels increased the sensitivity to TMZ, resulting in pronounced apoptosis. The increased sensitivity may be partly due to the low levels of GSH because only the *SLC7A11* over-expressing cells exhibited increased GSH production after treatment with TMZ. In addition, marked activation of caspase-3 in knock-down cells confirmed that suppression of *SLC7A11* facilitated TMZ-induced activation of the apoptotic pathway.

It may be that the *SLC7A11* knock-down cells exhibit the so-called "threshold concept for cancer therapy," whereby an additional increase in ROS levels by ROS-generating agents, such as chemotherapy drugs, pushes the endogenous levels of ROS past a cellular tolerability threshold (30). TMZ has also been shown to generate ROS in human glioblastoma cell lines, including superoxides, cytosolic H_2O_2, and mitochondrial H_2O_2, which could be suppressed by pretreatment with antioxidants resveratrol, vitamin C, and iron (31). Concurrent treatment of glioblastoma cell lines with TMZ and valproic acid (VPA), an anticonvulsant and mood-stabilizing drug, showed an increase in ROS and GSH depletion resulting in higher apoptosis compared to TMZ or VPA alone (32). These data suggest that redox regulation and TMZ-triggered ROS bursts can contribute to the sensitivity of glioma cells to chemotherapy. Indeed, the *SLC7A11* knock-down cells exhibited a significantly greater amount of endogenous ROS under basal conditions, and TMZ treatment augmented these levels because of impaired GSH production.

Recently, it has been shown that glioma chemoresistance to TMZ is linked to tighter mitochondrial coupling and low ROS production indicating that chemoresistance is related to a remodeling of the electron transport chain (17). Since mitochondrial respiration generates ROS, and system x_c^- has been shown to increase the antioxidant defense mechanisms to maintain redox balance, we hypothesized that *SLC7A11* levels in glioma may have an impact on mitochondrial health and function. Over-expression of *SLC7A11* in U251 glioma cells resulted in increased mitochondrial biogenesis and enhanced mitochondrial functions, indicated by increased mitochondrial membrane potential (Ψ_m). This was further confirmed by increased mRNA levels of several genes involved in mitochondrial biogenesis and function. While knock-down of *SLC7A11* did not impair mitochondrial respiration, over-expression of *SLC7A11* significantly increased the oxygen consumption rate (OCR) which is reflective of increased OXPHOS, and was accompanied by an increase in ATP generation. However, *SLC7A11* over-expressing U251 glioma generated less cytosolic and mitochondrial H_2O_2 compared to *SLC7A11* knock-down and control cells.

These results suggest that high expression of *SLC7A11* may play a role in mitochondrial biogenesis and energetics. How *SLC7A11* increases OXPHOS and the molecular signaling pathway involved have yet to be determined. The ability of cells to respond to stress is influenced by the energetic capacity of mitochondria, especially under conditions of increased energy demand. One possibility is that the *SLC7A11* over-expressing cells rely

more on oxidative phosphorylation due to an increased ATP demand. The generation of GSH relies on two ATP-dependent steps: synthesis of γ-glutamylcysteine and then subsequent addition of cysteine to the γ-glutamylcysteine. Thus, the *SLC7A11* over-expressing cells may rely on higher respiratory rates for GSH production. Alternatively, it may be that the increased GSH generation in the *SLC7A11* over-expressing cells prevents the accumulation of ROS-mediated defects in the mitochondria, thereby promoting enhanced mitochondrial respiration. Mitochondrial DNA has a high mutation rate and, as mtDNA mutations increase, the energy capacity of the cell declines until there is insufficient energy to sustain cellular function, indicating that the bioenergetic threshold of the cell has been reached (33). The molecular mechanisms involved and how the model of chemoresistance and mitochondria metabolism can be integrated warrants further examination. Whether other cancer cells that over-express *SLC7A11* have increased mitochondrial respiration and whether OXPHOS is dependent on system x_c^- remains to be explored. However, our observations provide a potential new link between system x_c^-, redox balance, and OXPHOS to promote glioma progression and survival.

In conclusion, we have shown that over-expression of system x_c^- in glioma confers a survival advantage suggesting worse prognosis in GBM patients. Indeed, strong xCT/*SLC7A11* expression in GBM patients correlated with an infiltrative phenotype on MRI and has been shown to be significantly associated with shorter progression-free and overall survival (34, 35). Microarray gene analysis of 60 human cancer cell lines used by the National Cancer Institute for drug screening (NCI-60) showed that *SLC7A11* expression was negatively correlated with sensitivity of tumor cells to anti-cancer drugs (4). Additionally, cytotoxic drugs have been shown to activate *SLC7A11* expression in various cancer cells (36). Our data shows that over-expression of *SLC7A11* not only promoted resistance to oxidative stress, but also implicated system x_c^- in TMZ resistance and altered metabolism in GBM. In U251 cells, over-expression of *SLC7A11* promoted increased GSH production under oxidative stress and genotoxic stress. The GSH neutralized intracellular ROS and increased the survival of the cells once stressed. Over-expression of *SLC7A11* was also correlated with an increased mitochondrial metabolism, which may contribute to the increased chemoresistance in these cells to TMZ. Additional studies are warranted to explore the molecular mechanisms involved in the *SLC7A11*-mediated drug resistance and determine whether *SLC7A11* may be a therapeutic target. Therefore, further investigation of manipulating the activity of this transporter either alone or in combination with other treatment modalities may lead to improved therapies and clinical outcomes of patients with GBM.

Supplementary Material

Refer to Web version on PubMed Central for supplementary material.

Acknowledgements

Works Cited

1. Brandes AA, Tosoni A, Spagnolli F, Frezza G, Leonardi M, Calbucci F, et al. Disease progression or pseudoprogression after concomitant radiochemotherapy treatment: pitfalls in neurooncology. Neuro Oncol 2008;10(3):361–7. 10.1215/15228517-2008-008. PubMed PMID: 18401015; PubMed Central PMCID: PMC2563059. [PubMed: 18401015]

2. Stupp R, Mason WP, van den Bent MJ, Weller M, Fisher B, Taphoorn MJ, et al. Radiotherapy plus concomitant and adjuvant temozolomide for glioblastoma. N Engl J Med 2005;352(10):987–96. 10.1056/NEJMoa043330. PubMed PMID: 15758009. [PubMed: 15758009]

3. Watkins S, Sontheimer H. Unique biology of gliomas: challenges and opportunities. Trends Neurosci 2012;35(9):546–56. 10.1016/j.tins.2012.05.001. PubMed PMID: 22683220; PubMed Central PMCID: PMC3578203. [PubMed: 22683220]

4. Huang Y, Dai Z, Barbacioru C, Sadee W. Cystine-glutamate transporter SLC7A11 in cancer chemosensitivity and chemoresistance. Cancer Res 2005;65(16):7446–54. 10.1158/0008-5472.CAN-04-4267. PubMed PMID: 16103098. [PubMed: 16103098]

5. Liou GY, Storz P. Reactive oxygen species in cancer. Free Radic Res 2010;44(5):479–96. 10.3109/10715761003667554. PubMed PMID: 20370557; PubMed Central PMCID: PMC3880197. [PubMed: 20370557]

6. Traverso N, Ricciarelli R, Nitti M, Marengo B, Furfaro AL, Pronzato MA, et al. Role of glutathione in cancer progression and chemoresistance. Oxid Med Cell Longev 2013;2013:972913 10.1155/2013/972913. PubMed PMID: 23766865; PubMed Central PMCID: PMC3673338. [PubMed: 23766865]

7. Trachootham D, Alexandre J, Huang P. Targeting cancer cells by ROS-mediated mechanisms: a radical therapeutic approach? Nat Rev Drug Discov 2009;8(7):579–91. 10.1038/nrd2803. PubMed PMID: 19478820. [PubMed: 19478820]

8. Chung WJ, Lyons SA, Nelson GM, Hamza H, Gladson CL, Gillespie GY, et al. Inhibition of cystine uptake disrupts the growth of primary brain tumors. J Neurosci 2005;25(31):7101–10. 10.1523/JNEUROSCI.5258-04.2005. PubMed PMID: 16079392; PubMed Central PMCID: PMC2681064. [PubMed: 16079392]

9. Ogunrinu TA, Sontheimer H. Hypoxia increases the dependence of glioma cells on glutathione. J Biol Chem 2010;285(48):37716–24. 10.1074/jbc.M110.161190. PubMed PMID: 20858898; PubMed Central PMCID: PMC2988376. [PubMed: 20858898]

10. Savaskan NE, Heckel A, Hahnen E, Engelhorn T, Doerfler A, Ganslandt O, et al. Small interfering RNA-mediated xCT silencing in gliomas inhibits neurodegeneration and alleviates brain edema. Nat Med 2008;14(6):629–32. doi: 10.1038/nm1772. PubMed PMID: 18469825. [PubMed: 18469825]

11. Singer E, Judkins J, Salomonis N, Matlaf L, Soteropoulos P, McAllister S, et al. Reactive oxygen species-mediated therapeutic response and resistance in glioblastoma. Cell Death Dis 2015;6:e1601 10.1038/cddis.2014.566. PubMed PMID: 25590811; PubMed Central PMCID: PMC4669764. [PubMed: 25590811]

12. Colvin OM, Friedman HS, Gamcsik MP, Fenselau C, Hilton J. Role of glutathione in cellular resistance to alkylating agents. Adv Enzyme Regul 1993;33:19–26. PubMed PMID: 8356908. [PubMed: 8356908]

13. Lo M, Wang YZ, Gout PW. The x(c)- cystine/glutamate antiporter: a potential target for therapy of cancer and other diseases. J Cell Physiol 2008;215(3):593–602. 10.1002/jcp.21366. PubMed PMID: 18181196. [PubMed: 18181196]

14. Lee HC, Kim DW, Jung KY, Park IC, Park MJ, Kim MS, et al. Increased expression of antioxidant enzymes in radioresistant variant from U251 human glioblastoma cell line. Int J Mol Med 2004;13(6):883–7. PubMed PMID: 15138630. [PubMed: 15138630]

15. Okuno S, Sato H, Kuriyama-Matsumura K, Tamba M, Wang H, Sohda S, et al. Role of cystine transport in intracellular glutathione level and cisplatin resistance in human ovarian cancer cell lines. Br J Cancer 2003;88(6):951–6. 10.1038/sj.bjc.6600786. PubMed PMID: 12644836; PubMed Central PMCID: PMC2377069. [PubMed: 12644836]

16. Lo M, Ling V, Wang YZ, Gout PW. The xc- cystine/glutamate antiporter: a mediator of pancreatic cancer growth with a role in drug resistance. Br J Cancer 2008;99(3):464–72. 10.1038/sj.bjc. 6604485. PubMed PMID: 18648370; PubMed Central PMCID: PMC2527809. [PubMed: 18648370]

17. Oliva CR, Moellering DR, Gillespie GY, Griguer CE. Acquisition of chemoresistance in gliomas is associated with increased mitochondrial coupling and decreased ROS production. PLoS One 2011;6(9):e24665 10.1371/journal.pone.0024665. PubMed PMID: 21931801; PubMed Central PMCID: PMC3170372. [PubMed: 21931801]

18. Brown CE, Starr R, Martinez C, Aguilar B, D'Apuzzo M, Todorov I, et al. Recognition and killing of brain tumor stem-like initiating cells by CD8+ cytolytic T cells. Cancer Res 2009;69(23):8886–93. 10.1158/0008-5472.CAN-09-2687. PubMed PMID: 19903840; PubMed Central PMCID: PMC2789196. [PubMed: 19903840]

19. Villeneuve LM, Reddy MA, Lanting LL, Wang M, Meng L, Natarajan R. Epigenetic histone H3 lysine 9 methylation in metabolic memory and inflammatory phenotype of vascular smooth muscle cells in diabetes. Proc Natl Acad Sci U S A 2008;105(26):9047–52. 10.1073/pnas. 0803623105. PubMed PMID: 18579779; PubMed Central PMCID: PMC2449362. [PubMed: 18579779]

20. Langmead B, Trapnell C, Pop M, Salzberg SL. Ultrafast and memory-efficient alignment of short DNA sequences to the human genome. Genome Biol 2009;10(3):R25 10.1186/gb-2009-10-3-r25. PubMed PMID: 19261174; PubMed Central PMCID: PMC2690996. [PubMed: 19261174]

21. Roberts A, Pachter L. Streaming fragment assignment for real-time analysis of sequencing experiments. Nat Methods 2013;10(1):71–3. 10.1038/nmeth.2251. PubMed PMID: 23160280; PubMed Central PMCID: PMC3880119. [PubMed: 23160280]

22. Anders S, Huber W. Differential expression analysis for sequence count data. Genome Biol 2010;11(10):R106 10.1186/gb-2010-11-10-r106. PubMed PMID: 20979621; PubMed Central PMCID: PMC3218662. [PubMed: 20979621]

23. Chou TC. Theoretical basis, experimental design, and computerized simulation of synergism and antagonism in drug combination studies. Pharmacol Rev 2006;58(3):621–81. 10.1124/pr.58.3.10. PubMed PMID: 16968952. [PubMed: 16968952]

24. Brand MD, Nicholls DG. Assessing mitochondrial dysfunction in cells. Biochem J 2011;435(2):297–312. 10.1042/BJ20110162. PubMed PMID: 21726199; PubMed Central PMCID: PMC3076726. [PubMed: 21726199]

25. Conrad M, Sato H. The oxidative stress-inducible cystine/glutamate antiporter, system x (c) (−) : cystine supplier and beyond. Amino Acids 2012;42(1):231–46. 10.1007/s00726-011-0867-5. PubMed PMID: 21409388. [PubMed: 21409388]

26. Chen L, Li X, Liu L, Yu B, Xue Y, Liu Y. Erastin sensitizes glioblastoma cells to temozolomide by restraining xCT and cystathionine-gamma-lyase function. Oncol Rep 2015;33(3):1465–74. 10.3892/or.2015.3712. PubMed PMID: 25585997. [PubMed: 25585997]

27. Robe PA, Bentires-Alj M, Bonif M, Rogister B, Deprez M, Haddada H, et al. In vitro and in vivo activity of the nuclear factor-kappaB inhibitor sulfasalazine in human glioblastomas. Clin Cancer Res 2004;10(16):5595–603. 10.1158/1078-0432.CCR-03-0392. PubMed PMID: 15328202. [PubMed: 15328202]

28. Pham AN, Blower PE, Alvarado O, Ravula R, Gout PW, Huang Y. Pharmacogenomic approach reveals a role for the x(c)- cystine/glutamate antiporter in growth and celastrol resistance of glioma cell lines. J Pharmacol Exp Ther 2010;332(3):949–58. 10.1124/jpet.109.162248. PubMed PMID: 20007406. [PubMed: 20007406]

29. Robe PA, Martin DH, Nguyen-Khac MT, Artesi M, Deprez M, Albert A, et al. Early termination of ISRCTN45828668, a phase 1/2 prospective, randomized study of sulfasalazine for the treatment of progressing malignant gliomas in adults. BMC Cancer 2009;9:372 10.1186/1471-2407-9-372. PubMed PMID: 19840379; PubMed Central PMCID: PMC2771045. [PubMed: 19840379]

30. Gupta SC, Hevia D, Patchva S, Park B, Koh W, Aggarwal BB. Upsides and downsides of reactive oxygen species for cancer: the roles of reactive oxygen species in tumorigenesis, prevention, and therapy. Antioxid Redox Signal 2012;16(11):1295–322. 10.1089/ars.2011.4414. PubMed PMID: 22117137; PubMed Central PMCID: PMC3324815. [PubMed: 22117137]

31. Lin CJ, Lee CC, Shih YL, Lin TY, Wang SH, Lin YF, et al. Resveratrol enhances the therapeutic effect of temozolomide against malignant glioma in vitro and in vivo by inhibiting autophagy. Free Radic Biol Med 2012;52(2):377–91. 10.1016/j.freeradbiomed.2011.10.487. PubMed PMID: 22094224. [PubMed: 22094224]

32. Chen RS, Song YM, Zhou ZY, Tong T, Li Y, Fu M, et al. Disruption of xCT inhibits cancer cell metastasis via the caveolin-1/beta-catenin pathway. Oncogene 2009;28(4):599–609. 10.1038/onc. 2008.414. PubMed PMID: 19015640. [PubMed: 19015640]

33. Wallace DC. Mitochondria and cancer. Nat Rev Cancer 2012;12(10):685–98. 10.1038/nrc3365. PubMed PMID: 23001348; PubMed Central PMCID: PMC4371788. [PubMed: 23001348]

34. Takeuchi S, Wada K, Toyooka T, Shinomiya N, Shimazaki H, Nakanishi K, et al. Increased xCT expression correlates with tumor invasion and outcome in patients with glioblastomas. Neurosurgery 2013;72(1):33–41; 10.1227/NEU.0b013e318276b2de. PubMed PMID: 23096413.

35. Robert SM, Buckingham SC, Campbell SL, Robel S, Holt KT, Ogunrinu-Babarinde T, et al. SLC7A11 expression is associated with seizures and predicts poor survival in patients with malignant glioma. Sci Transl Med 2015;7(289):289ra86 10.1126/scitranslmed.aaa8103. PubMed PMID: 26019222; PubMed Central PMCID: PMC4503260.

36. Banjac A, Perisic T, Sato H, Seiler A, Bannai S, Weiss N, et al. The cystine/cysteine cycle: a redox cycle regulating susceptibility versus resistance to cell death. Oncogene 2008;27(11):1618–28. 10.1038/sj.onc.1210796. PubMed PMID: 17828297. [PubMed: 17828297]

37. Berriz GF, Beaver JE, Cenik C, Tasan M, Roth FP. Next generation software for functional trend analysis. Bioinformatics 2009;25(22):3043–4. 10.1093/bioinformatics/btp498. PubMed PMID: 19717575; PubMed Central PMCID: PMC2800365. [PubMed: 19717575]
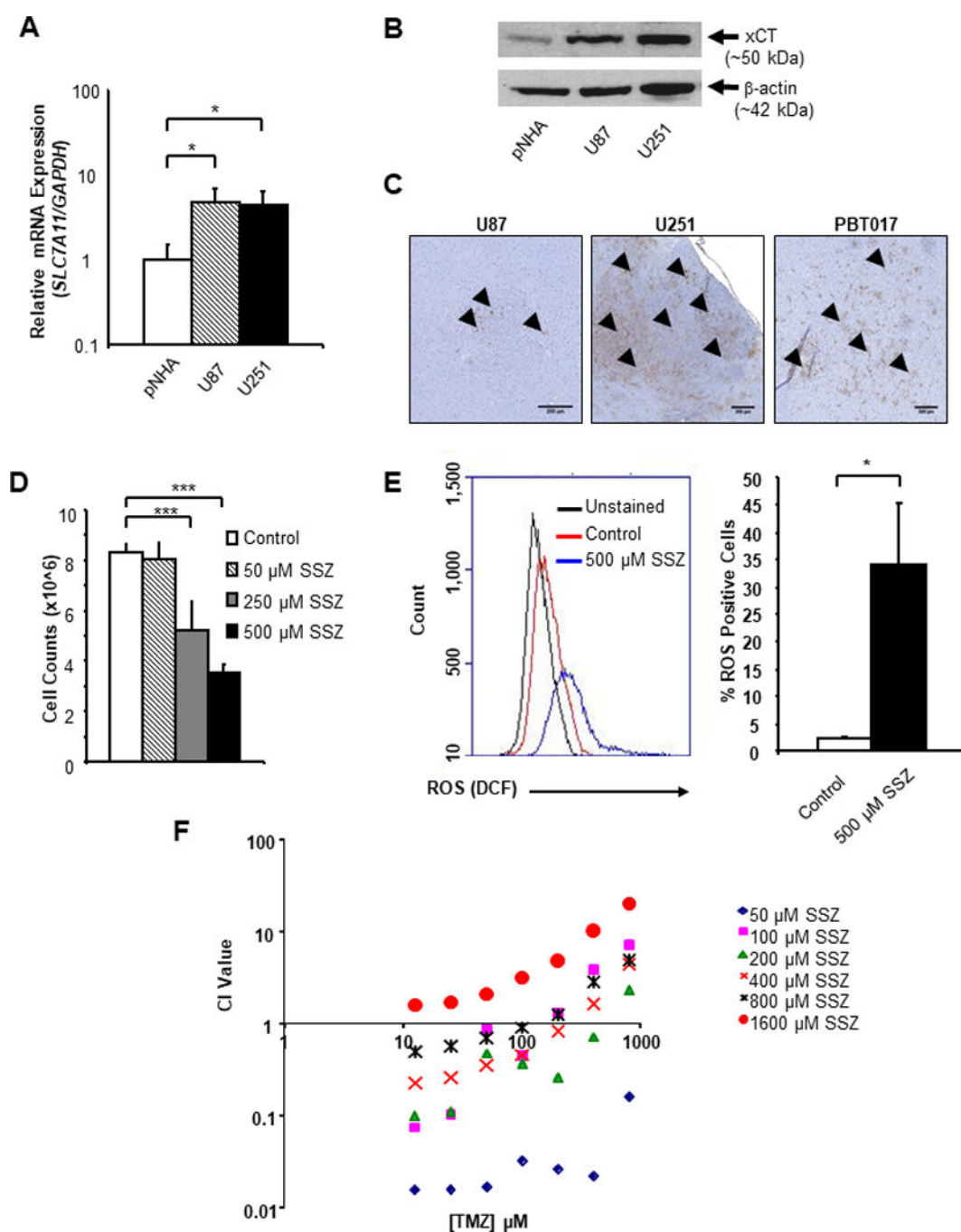
Fig. 1.
SLC7A11/xCT is up-regulated in glioma cell lines in which inhibition of system x_c^- modulates cell survival and proliferation. (A) Real-time quantitative RT-PCR analysis of *SLC7A11* expression in human U87 and U251 glioma cell lines compared to primary normal human astrocytes (pNHA). (B) Immunoblot analysis of xCT and β-actin (loading control) expression in U87 and U251 glioma cells compared to pNHAs. (C) Immunohistochemical staining for xCT in the orthotopic tumors; positive xCT staining indicated by arrows. Scale bar, 200 μm. (D) Proliferation of U251 cells treated with

increasing doses of sulfasalazine (SSZ) for 72 h. (E) Intracellular ROS levels in U251 cells treated with or without (control) 500 µM SSZ for 72 h. Error bars indicate SD; *, $P<0.05$; **, $P<0.01$; ***, $P<0.001$. (F) Combination indices (CI) of U251 glioma cells treated with SSZ (50, 100, 200, 400, 800 or 1600 µM) and increasing doses of TMZ (12.5, 25, 50, 100, 200, 400, 800 µM) to determine drug interactions. CI<1, +1, and >1 indicate synergism, additive effect, and antagonism, respectively.
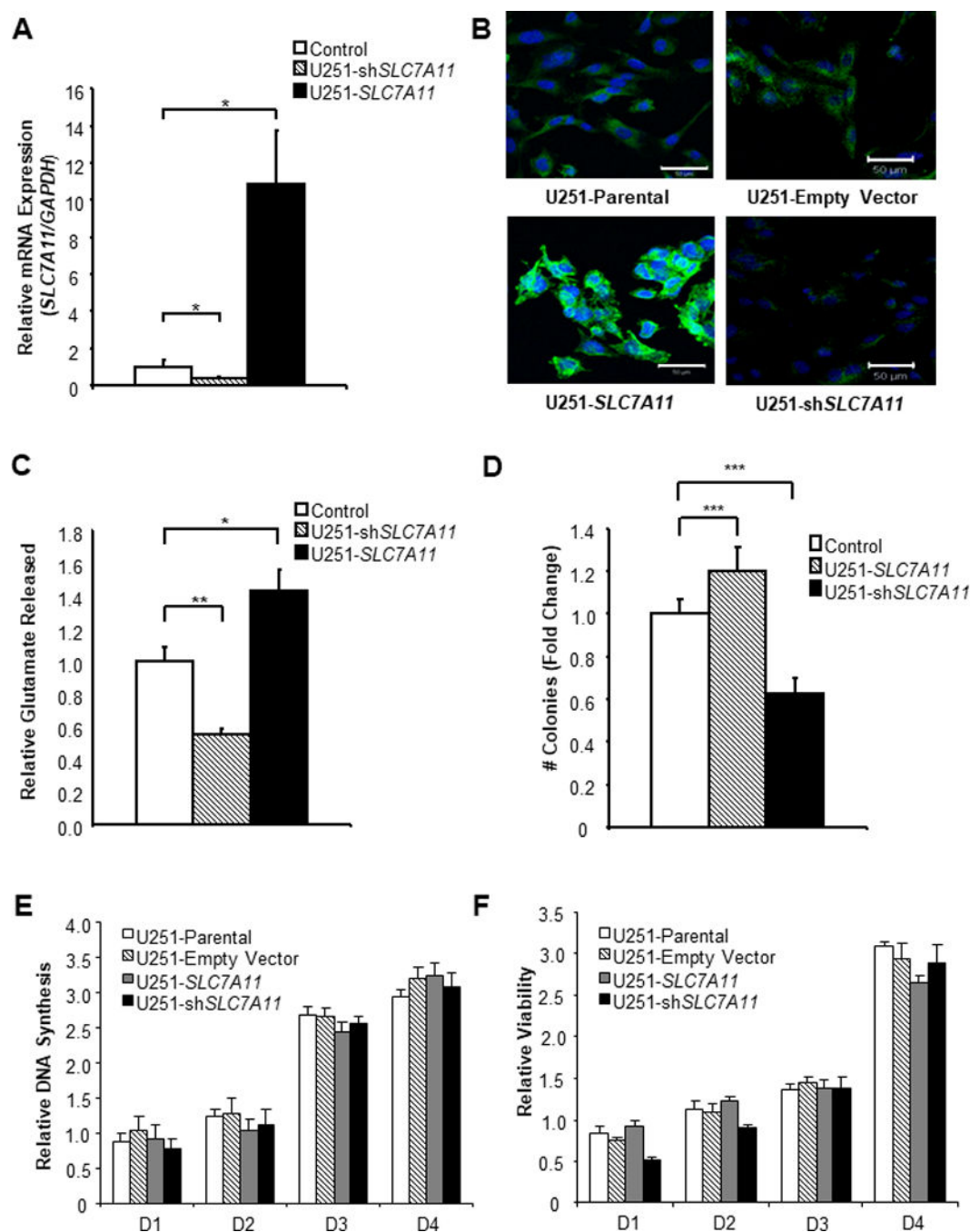
Fig. 2.

Viability and proliferation are not affected in stable *SLC7A11*-knock-down and over-expressing U251 glioma cells. (A) Quantification of xCT (*SLC7A11*) mRNA in U251 glioma transduced with viral vector containing *SLC7A11* over-expression construct or viral vector containing sh*SLC7A11* (TRCN0000043126). (B) Confocal microscopy images of *SLC7A11* over-expression and knock-down U251 cell lines stained for xCT protein (green). Cells were counterstained with DAPI (blue) to visualize nuclei. Scale bars, 50 μm. (C) Amount of glutamate released into the media by *SLC7A11* over-expressing and knock-down

U251 cell lines relative to control. (D) Quantification of anchorage-independent cell growth in *SLC7A11*-modified glioma cells compared to controls. (E) Proliferation of *SLC7A11*-modified glioma cells at indicated time-points as measured by BrdU incorporation. (F) Viability of *SLC7A11*-modified glioma cells measured by CCK-8 assay at indicated time-points. Data shown are means from a representative experiment. Error bars indicate SD; *, P<0.05; **, P<0.01; ***, P<0.001.
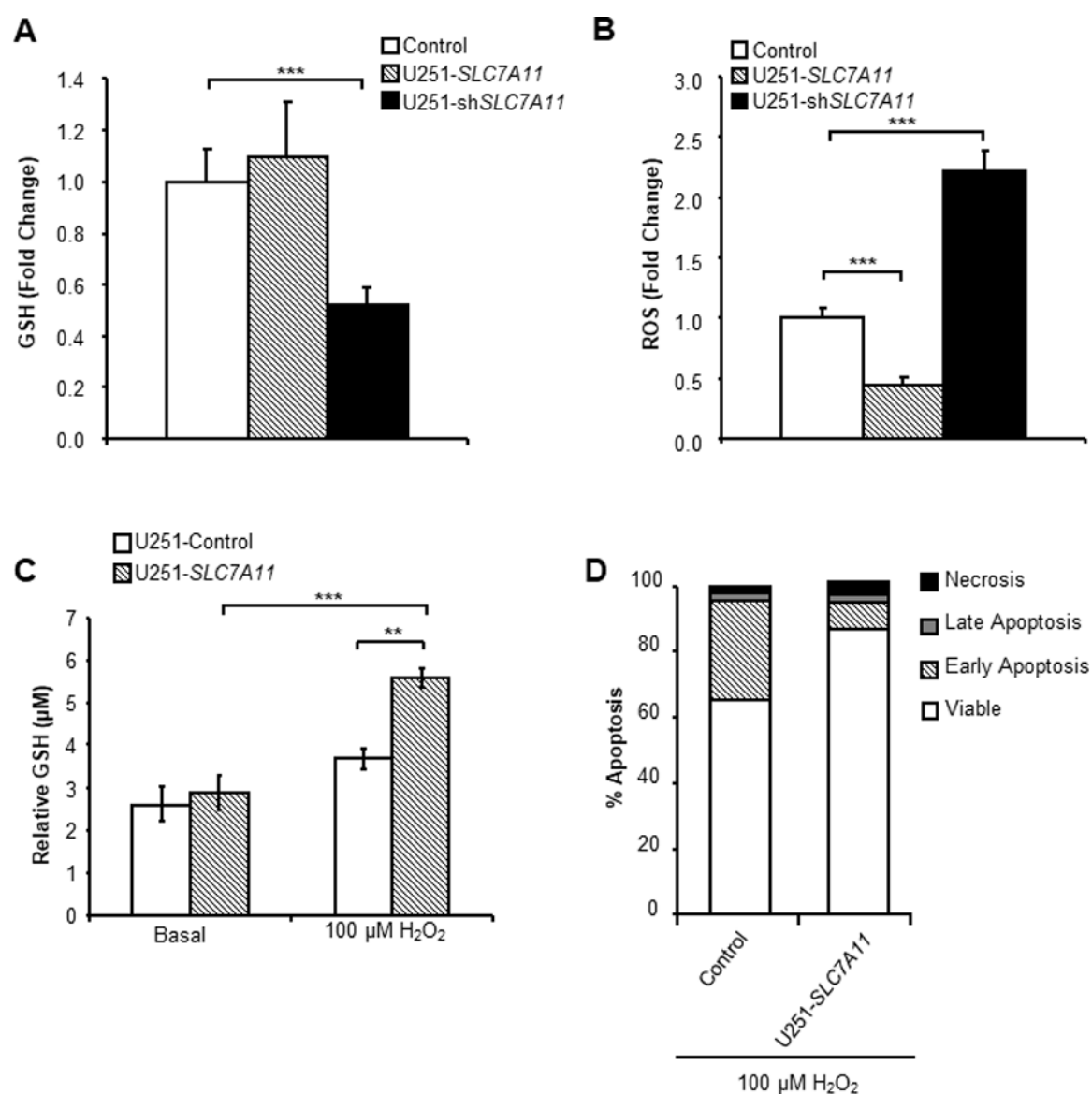
Fig. 3.

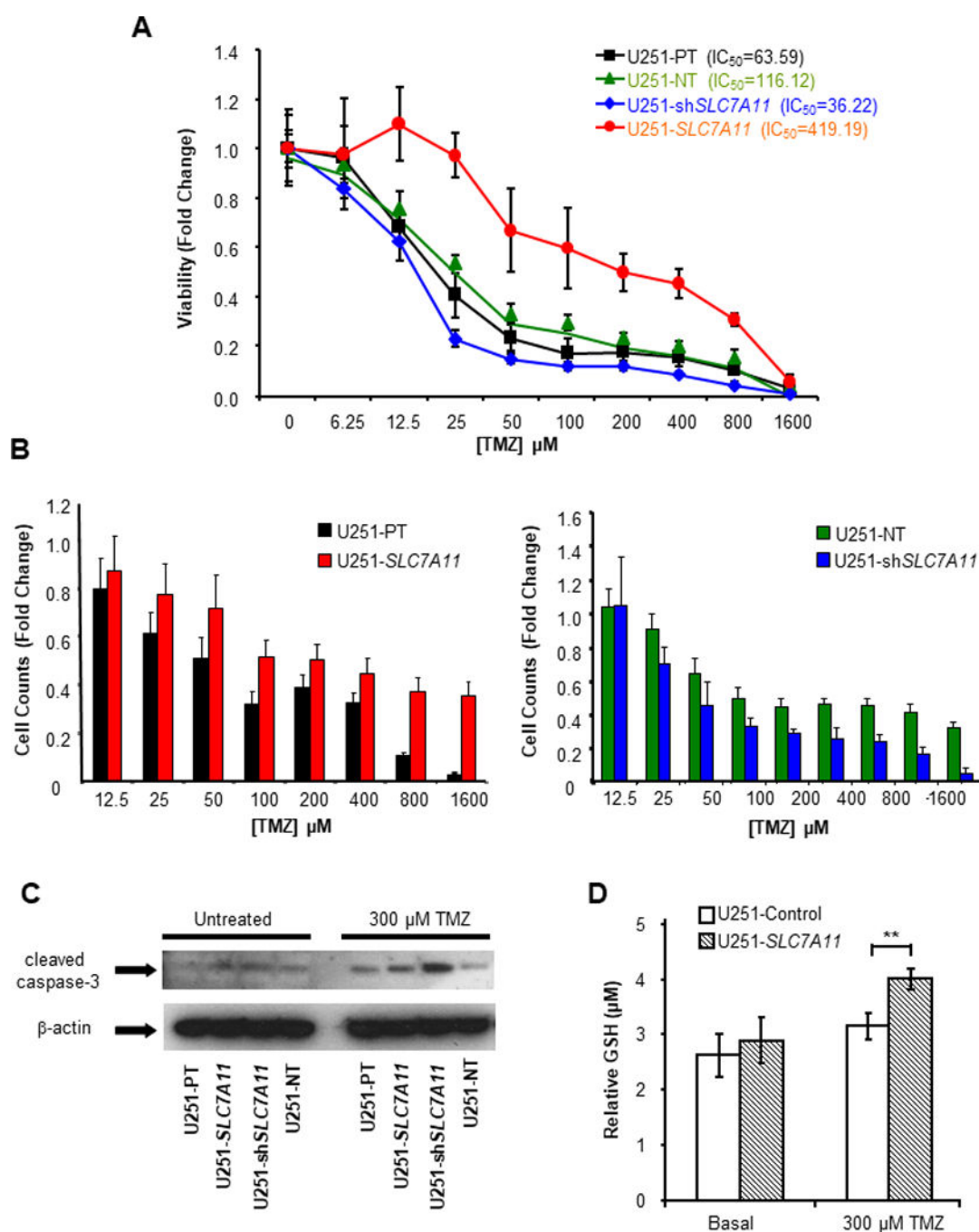*SLC7A11* over-expressing U251 glioma cells are more resistant to oxidative stress. (A) Relative intracellular glutathione (GSH) measured in *SLC7A11*-modified U251s under normal culture conditions. (B) Relative intracellular ROS measured in *SLC7A11*-modified U251s under normal culture conditions. (C) Relative intracellular GSH measured in *SLC7A11* over-expressing U251 glioma after 6 h treatment with 100μM H_2O_2. (D) Flow cytometry analysis of Annexin V/propidium iodide staining of *SLC7A11* over-expressing and control glioma after 6 h treatment with 100 μM H_2O_2. Data shown in (A), (B) and (C) are means from a representative experiment. Error bars indicate SD; *, P<0.05; **, P<0.01; ***, P<0.001.

Fig. 4.

SLC7A11 over-expression in U251 glioma conferred increased resistance to TMZ. (A) Viability of *SLC7A11* over-expressing and knock-down U251 cells treated for 72 h with increasing doses of TMZ (IC_{50} values are indicated). (B) Proliferation of *SLC7A11* over-expressing and knock-down U251 cells treated for 72 h with increasing doses of TMZ compared to respective controls. (C) Immunoblot analysis of cleaved caspase-3 and β-actin (loading control) in *SLC7A11*-modified U251 and respective control cells after treatment with 300 μM TMZ. (D) Relative intracellular GSH in *SLC7A11* over-expressing U251 cells

after treatment with 300 μM TMZ for 72 h. Data shown are means from a representative experiment. Error bars indicate SD; *, P<0.05; **, P<0.01; ***, P<0.001.
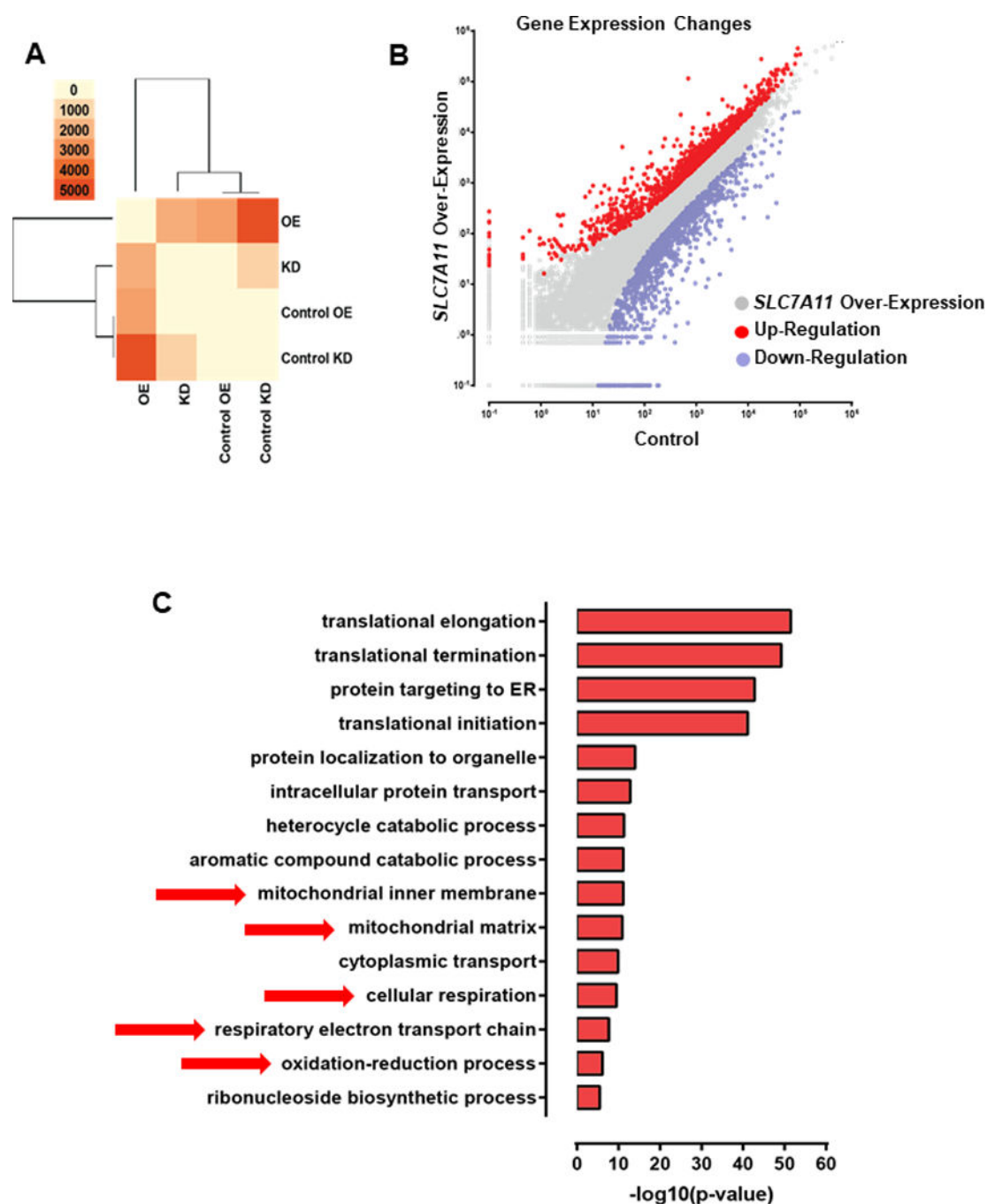
Fig. 5.
Gene expression changes upon *SLC7A11* over-expression and knock-down in U251 cells.
(A) Global similarity of gene expression profiles between *SLC7A11* over-expression (OE),
knock-down (KD) and matched control samples. Differential expression analysis was carried
out on biological replicate samples for all pairs of conditions using DESeq (22); the heatmap
shows the number of differential genes, which was used as a similarity metric between
conditions. (B) Differentially expressed genes between *SLC7A11* over-expressing and
control U251 cells. (C) Representative Gene Ontology (GO) terms enriched in genes up-

regulated upon *SLC7A11* over-expression in U251 cells. GO enrichment analysis was carried out using FuncAssociate (37). Complete lists of enriched categories are provided in the Supplementary Data.
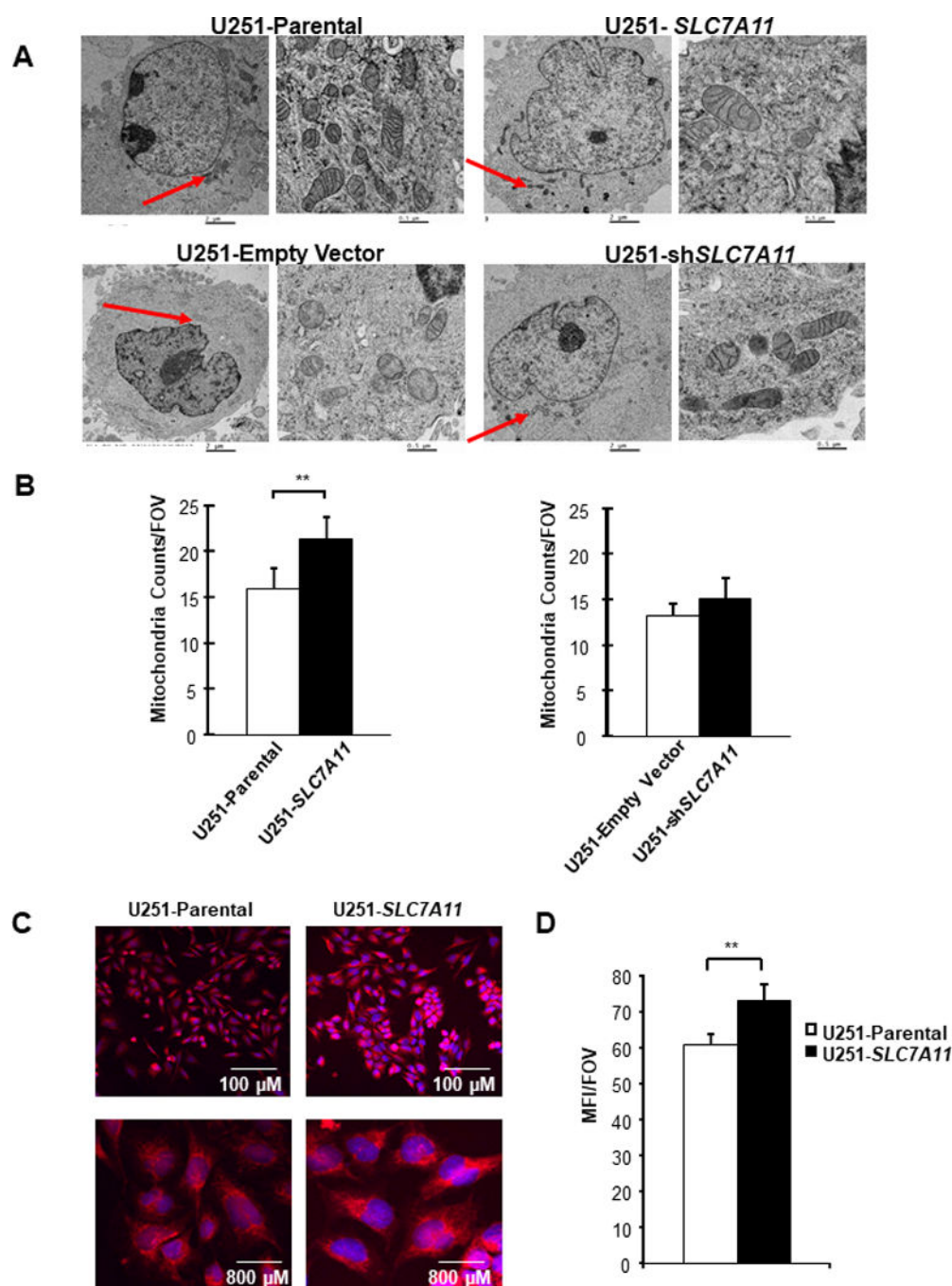
Fig. 6.

SLC7A11 over-expressing U251 glioma has increased mitochondrial biogenesis and increased mitochondrial membrane potential. (A) Transmission electron micrographs of *SLC7A11*-modified glioma cells and control cells. Representative mitochondria are indicated by a red arrow. Scale bars: 2 um (left micrograph) and 0.5 um (right micrograph) of each set. (B) Quantification of mitochondria per field of view (FOV) in *SLC7A11* modified lines compared to their respective controls. (C) Fluorescent microscopic examination of the Ψ_m-dependent uptake and retention of MitoTracker Red CMXRos into

mitochondria in *SLC7A11* over-expressing glioma compared to parental control. Scale bars: 100 μm. (D) Quantification of the mean fluorescent intensity (MFI) per field of view (FOV) of MitoTracker Red CMXRos staining in the *SLC7A11* over-expressing glioma compared to control cells. Data shown in (B) and (D) are means from a representative experiment. Error bars indicate SD; *, P<0.05; **, P<0.01.
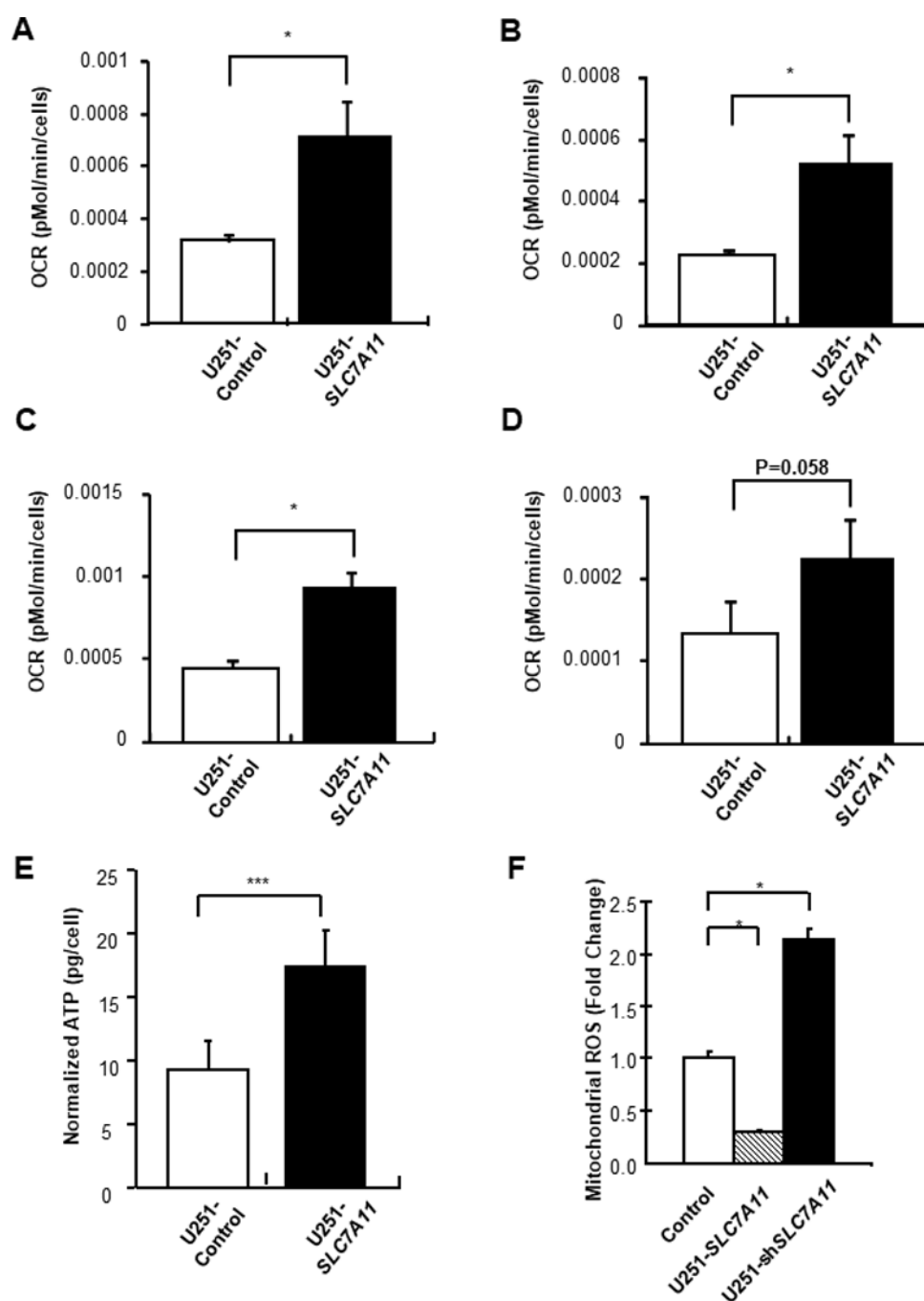
Fig. 7.
Oxygen Consumption Rates (OCR) and respiration parameters in *SLC7A11* over-expressing U251 glioma cells compared to parental U251 cells. (A) Baseline Respiratory Capacity (B) ATP-linked Respiration and (C) Maximal Respiratory Capacity and (D) Reserve Capacity calculated for the *SLC7A11* over-expressing glioma compared to parental U251 cells. (E) Intracellular ATP normalized to cell number in *SLC7A11* over-expressing glioma cells compared to control cells. (F) Mitochondrial ROS measured in *SLC7A11*-modified glioma cells by the MitoTracker Red CM-H$_2$XRos dye which stains actively respiring cell,

accumulates in the mitochondria and is dependent on the mitochondria membrane potential. Error bars indicate SD; *, P<0.05; **, P<0.01; ***, P<0.001.